PHYSICAL REVIEW D **95,** 023526 (2017)

Spacetime dynamics of a Higgs vacuum instability during inflation

William E. East,[1,2] John Kearney,[3] Bibhushan Shakya,[4] Hojin Yoo,[5] and Kathryn M. Zurek[5]
[1]*Kavli Institute for Particle Astrophysics and Cosmology, Stanford University, SLAC National Accelerator Laboratory, Menlo Park, California 94025, USA*
[2]*Perimeter Institute for Theoretical Physics, Waterloo, Ontario N2L 2Y5, Canada*
[3]*Theoretical Physics Department, Fermi National Accelerator Laboratory, Batavia, Illinois 60510, USA*
[4]*Michigan Center for Theoretical Physics, University of Michigan, Ann Arbor, Michigan 48019, USA*
[5]*Theory Group, Lawrence Berkeley National Laboratory and Berkeley Center for Theoretical Physics, University of California, Berkeley, California 94709, USA*
(Received 25 July 2016; published 31 January 2017)

A remarkable prediction of the Standard Model is that, in the absence of corrections lifting the energy density, the Higgs potential becomes negative at large field values. If the Higgs field samples this part of the potential during inflation, the negative energy density may locally destabilize the spacetime. We use numerical simulations of the Einstein equations to study the evolution of inflation-induced Higgs fluctuations as they grow towards the true (negative-energy) minimum. These simulations show that forming a single patch of true vacuum in our past light cone during inflation is incompatible with the existence of our Universe; the boundary of the true vacuum region grows outward in a causally disconnected manner from the crunching interior, which forms a black hole. We also find that these black hole horizons may be arbitrarily elongated—even forming black strings—in violation of the hoop conjecture. By extending the numerical solution of the Fokker-Planck equation to the exponentially suppressed tails of the field distribution at large field values, we derive a rigorous correlation between a future measurement of the tensor-to-scalar ratio and the scale at which the Higgs potential must receive stabilizing corrections in order for the Universe to have survived inflation until today.

DOI: 10.1103/PhysRevD.95.023526

I. INTRODUCTION

A striking feature of the Standard Model (SM) is that, in the absence of stabilizing corrections, the Higgs potential develops an instability, with the maximum of the potential occurring at $V(\Lambda_{\rm max})^{1/4} \sim 10^{10}$ GeV. This leads to the existence of a "true vacuum" at large Higgs field values, which may carry important consequences for our Universe [1–11]. Our present existence does not necessarily demand physics beyond the SM, since current measurements of the Higgs boson and top quark masses indicate that the electroweak (EW) vacuum is metastable, i.e., long-lived relative to the age of the Universe. The scenario is different, however, if our Universe underwent an early period of cosmic inflation with substantial energy density. The inflaton energy density, parametrized by the Hubble parameter H, produces large local fluctuations in the Higgs field, $\delta h \sim \frac{H}{2\pi}$. As such, when H is sufficiently large during inflation, the Higgs field may sample the unstable part of the potential.

If sampling this part of the potential can be shown to be catastrophic for the surrounding spacetime, the eventual survival of our Universe in the EW vacuum would consequently imply constraints on the nature of the inflationary epoch that gave rise to our Universe. Conversely, near-future cosmic microwave background experiments will probe tensor-to-scalar ratios of $r \gtrsim 0.002$ [12], corresponding to inflationary scales $H > 10^{13}$ GeV. If it can be shown that the SM Higgs potential is inconsistent with such high-scale inflation, a measurement of nonzero r provides evidence for the existence of stabilizing corrections to the Higgs potential.

In recent years, the interplay between the SM Higgs potential instability and inflation has received significant attention [13–24]. A complete treatment of this problem has two important aspects: first, the evolution of the Higgs field under a combination of (inflation-induced) quantum fluctuations and the classical potential and, second, the evolution of spacetime responding to the Higgs vacuum.

Initial groundwork on the first aspect was laid in Ref. [13], which employed a stochastic, Fokker-Planck (FP) approach to study the evolution and distribution of Higgs fluctuations in Hubble-sized patches during inflation. While this is a suitable approach incorporating both leading classical and quantum effects, the analysis of [13] was predicated on the assumption that fluctuations exceeding $\Lambda_{\rm max}$ rapidly transitioned to the true vacuum and disappeared, resulting in a miscalculation of the distribution. It was subsequently shown in [17], however, that fluctuations continue to evolve in an inflationary background well past the point where the Higgs quartic becomes negative. In fact, it is the formation of fluctuations well beyond $\Lambda_{\rm max}$ that carry the most significant implications for our Universe, making it necessary to study the full distribution of fluctuations. As Ref. [23] later demonstrated, a true vacuum patch capable of backreacting on the inflating spacetime only forms at about the time that a

fluctuation becomes sufficiently large that the Higgs field locally exits the slow-roll regime.

The first meaningful investigation of the second aspect—the response of the spacetime to the Higgs vacuum evolution—appeared in Ref. [24].[1] In order to make the study analytically tractable, they adopted an idealized setup of a spherically symmetric thin-wall anti–de Sitter (AdS) bubble in a de Sitter (dS) background and found that true vacuum bubbles persist throughout inflation for realistic parameters. As such, the formation of a single such true vacuum patch in our past light cone during inflation would be disastrous for our Universe—after inflation, such patches would expand and destroy the surrounding space in the EW vacuum.[2]

The main goal of this paper is a comprehensive study of both aspects, the field evolution and subsequent reaction of the spacetime. We improve the study of the former aspect by numerically resolving the full probability distribution of Higgs fluctuations in the FP equation, even into the exponentially suppressed tails that govern single patches in our past light cone. This is in contrast to previous studies [13,17,24], which relied on a type of "matching" procedure between quantum-dominated and classical-dominated evolution in the FP treatment.[3] We carry out a comprehensive study of the second aspect by employing full numerical solutions to the Einstein equations instead of the thin-wall approximation.

Moving beyond the approximations previously employed in the literature is vital to providing a complete description of the interplay between inflation and the Higgs field for several reasons. First, a more complete numerical solution to the FP equation allows us to fully capture the important effects of the renormalization group-improved potential, as well as the crucial non-Gaussian tails of the Higgs field value distribution. In particular, as Ref. [23] argued based on the Higgs effective potential in dS space calculated in [19] and Wilsonian effective field theory, an appropriate scale at which to evaluate the Higgs self-coupling is $\mu \simeq \sqrt{H^2 + h^2}$ as opposed to $\mu \simeq |h|$. This choice minimizes large logarithms and incorporates the relevant energy scale from inflation. As we shall see, fully including the effects of the renormalization group-improved potential influences both small and large fluctuations. Meanwhile, as we demonstrate, it is the exponentially suppressed but long tails of the distribution that ultimately determine the rate at which true vacuum patches form.

Second, since the evolution of a Higgs fluctuation becomes classical well before becoming sufficiently large to backreact on the spacetime, it is important to study a patch rapidly evolving to the true vacuum, gaining significant energy as it falls, as a dynamical general relativity process. The thin-wall approximation employed in [24] is valid when fluctuations beyond the potential barrier at $\Lambda_{\max}$ occur via a Coleman–de Luccia tunneling process [27], resulting in a true vacuum bubble interior that rapidly transitions to false vacuum exterior across a thin boundary. During inflation, however, Higgs fluctuations are more appropriately described by a broad, Hubble-sized variation in the field, more akin to a Hawking-Moss instanton [28] (see [17] for a detailed discussion). Here we will not make any simplifying assumptions regarding the Higgs fluctuation being a region of AdS separated from the surround dS at an infinitely thin bubble wall, though we will still use the term "bubble" to refer to dynamically formed regions where the Higgs field is near the true vacuum. Our numerical simulations allow us to study the full behavior of extended fluctuations, offering the first in-depth understanding of the field and spacetime dynamics of these Higgs fluctuations.

In particular, we highlight three important aspects of true vacuum patch formation. First, we show that patches only rapidly diverge to the true vacuum and backreact on the inflating spacetime once the Higgs field locally exits the slow-roll regime. Second, the associated large negative energy density does terminate inflation locally, eventually producing a crunching region, but this region is hidden behind a black hole horizon that is surrounded by an expanding shell of negative energy density. Third, for reasonable parameters, the shell of negative energy density expands into the surrounding spacetime in a manner causally disconnected from the crunching interior, in contrast to the thin-wall AdS bubble. As a result, its growth is not sensitive to the crunching behavior of the spacetime in the interior, allowing such true vacuum regions to persist through inflation.

We thus confirm that the formation of a single, sufficiently large fluctuation during inflation precludes the existence of our Universe, resulting in a bound $H/\Lambda_{\max} \lesssim 0.07$ that, once a number of competing effects are taken into account, is similar to that found in previous studies [17,24]. In addition, our numerical approach enables us to study more complicated nonspherical solutions, where we find that the formation of AdS-like regions from the field falling to the true minimum at negative potential energy allows for the formation of black holes with arbitrarily elongated

[1]Earlier studies did not investigate the reaction of the spacetime, instead assuming a variety of outcomes. For example, [13] assumed that fluctuations to the true vacuum only locally terminate inflation, rapidly forming AdS regions that "benignly" crunch (shrinking to negligible volume), while [15,21] supposed a single true vacuum patch in our past light cone eventually devours all of spacetime. Reference [17] considered both extreme possibilities.

[2]See also [25,26] for related working on the collision of crunching bubbles.

[3]This matching procedure consists of using the FP equation to track the field evolution to the point where classical effects start to dominate over quantum effects, and switching to the classical equation of motion beyond this point (thus ignoring the quantum effects) to track the subsequent evolution.

horizons (and black strings), in violation of the hoop conjecture [29].

We emphasize that, while the presence of new physics at the weak scale could substantially change the quantitative features of the Higgs evolution due to the modified Higgs potential, there are many conceptual points in the interplay between an inflating spacetime and a field with a vacuum instability that are applicable in a wider context. Furthermore, we illustrate in this work some of the qualitatively different features that Einstein gravity exhibits in the presence of negative energy density, including the formation of black holes with arbitrarily elongated horizons, or even black strings, that hide the crunching regions from outside observers. These touch on fundamental considerations in gravity such as the topology of black hole horizons, the hoop conjecture, and cosmic censorship.

The rest of this paper is organized as follows. In Sec. II, we briefly review the stochastic approach to studying the evolution of Higgs field fluctuations using the FP equation. Section III is the main part of this paper where, using full numerical simulations, we study the spacetime dynamics of the patches exhibiting large fluctuations that evolve to the true vacuum. In Sec. IV, we present a complete numerical solution of the FP equation, allowing us to extract constraints on the Hubble scale or the form of the Higgs potential from the survival of our Universe through inflation. Finally, we summarize our conclusions in Sec. V.

II. EVOLUTION OF THE HIGGS FIELD DURING INFLATION

To set the stage for studying the evolution of spacetime in response to unstable Higgs fluctuations in the next section, here we review the evolution of the Higgs field during inflation and the formation of large fluctuations as modeled by the Fokker-Planck (FP) equation. We restrict ourselves here to providing the context; a more quantitative numerical solution of the FP equation and in-depth discussion will be presented later in Sec. IV.

When $H^2 \gtrsim V''(\Lambda_{\rm max})$, where $V(\Lambda_{\rm max})$ is the maximum of the potential, a statistical approach can be utilized for studying the Higgs evolution during inflation via the Fokker-Planck (FP) equation [13,30,31],

$$\frac{\partial P}{\partial t} = \frac{\partial}{\partial h}\left[\frac{V'(h)}{3H}P + \frac{H^3}{8\pi^2}\frac{\partial P}{\partial h}\right]. \tag{1}$$

This equation governs the probability distribution $P(h,t)$ corresponding to the average field value h in a patch of size $\sim H^{-1}$ at time t. The second moment of the distribution, $\langle h^2\rangle = \int dh h^2 P(h,t)$, reproduces well the behavior obtained from the equation of motion for $\langle h^2\rangle$ in the Gaussian approximation with subhorizon modes integrated out, at least for small fluctuations (see, e.g., [23,32]).[4]

The first term on the right of Eq. (1) accounts for classical evolution due to the potential in the slow-roll approximation. As argued in Ref. [23], since the FP equation describes the evolution of Higgs fluctuations on scales $R \gtrsim H^{-1}$, the potential V appearing in Eq. (1) is an effective potential containing only superhorizon modes. Mode functions of non-Higgs SM fields (fermions and gauge bosons) rapidly decay outside the horizon, so these fields do not correct this infrared/superhorizon Higgs effective potential. However, they do renormalize the quartic coupling in the ultraviolet (UV). As such, the appropriate potential is

$$V(h) = \frac{\lambda(\mu)}{4}h^4, \tag{2}$$

where h is the canonically normalized Higgs field and at leading order $\lambda(\mu)$ is the RG-improved quartic, matched to the UV quartic (taken to be the SM quartic as in Minkowski space) at the scale at which the SM fields decouple. Taking the Higgs-dependent mass into account, the optimal choice of scale is $\mu \simeq \sqrt{H^2+h^2}$ [19,23]—for small fluctuations, this corresponds to the infrared cutoff $\mu \simeq H$ below which subhorizon physics is integrated out [33]. We assume for the time being that the Higgs has no corrections to Eq. (2) from, e.g., a coupling to gravity of the form H^2h^2; we return to the impact of such a term in Sec. IV B.

The second term in Eq. (1) corresponds to the quantum-to-classical transition experienced by field modes during inflation as a result of horizon crossing. The result is a random walk for h with steps of order $\sim\frac{H}{2\pi}$ as subsequent modes cross the horizon. These steps can also be thought of as thermal fluctuations in an inflationary background with a Gibbons-Hawking temperature $\frac{H}{2\pi}$ [34], which increase or decrease the size of a local fluctuation depending on whether the modes crossing the horizon add coherently or destructively with the longer wavelength modes that froze out earlier. Thus the characteristic size of the spatial field structure induced by such fluctuations is $\sim H^{-1}$.

Initially, evolution is dominated by quantum fluctuations via the second term. This causes large local fluctuations in the Higgs field that, for sufficiently large H, may result in the field locally sampling the unstable part of the potential, $|h| \gtrsim \Lambda_{\rm max}$. Though a positive quartic may somewhat suppress the growth of fluctuations for $\sqrt{H^2+h^2} \lesssim \Lambda_{\rm max}$, the classical effect due to the unstable potential causes the distribution to grow somewhat more quickly once $\sqrt{H^2+h^2} \gtrsim \Lambda_{\rm max}$. At this point, the stochastic term still

[4]For a discussion of the regime of validity of this equation for inflationary evolution of the Higgs (as opposed to a Coleman–de Lucia or Hawking-Moss instanton solution), we refer the interested reader to Ref. [17].

dominates over the classical potential, so that a fluctuation does not yet grow inexorably toward the true vacuum. This only happens once the classical potential comes to dominate over quantum effects, when $|h| \gtrsim h_{\rm cl}$, where

$$V'(h_{\rm cl}) = -\frac{3H^3}{2\pi}, \qquad h_{\rm cl} \approx H\left(\frac{3}{-2\pi\lambda}\right)^{1/3}, \tag{3}$$

i.e., when the slow-roll evolution due to the potential, $\dot{h}\Delta t \simeq V'(h_{\rm cl})/(3H^2)$, exceeds the stochastic evolution due to inflationary fluctuations. From this point, as described in [17], the field necessarily diverges to the true vacuum.

However, as first emphasized in [23], the local energy density at this point is still overwhelmingly dominated by the inflationary energy density. Due to Hubble friction, the field continues to undergo slow-roll evolution, and a significant number of e-folds must pass after entering the classical regime, Eq. (3), until the Higgs exits the slow-roll regime. Meanwhile, inflation proceeds unabated. This regime is therefore still well described by the Fokker-Planck equation. It is only after a fluctuation becomes very large, $|h| \gtrsim h_{s/r}$, where

$$h_{s/r} = -\frac{V'(h_{s/r})}{3H^2} \approx H\left(\frac{3}{-\lambda}\right)^{1/2}, \tag{4}$$

that the slow-roll approximation breaks down, and the fluctuation rapidly diverges to the true vacuum. Only then does the energy density in the Higgs field become sufficiently large to backreact on the spacetime—we will explore this backreaction in the subsequent section. Consequently, to determine the fraction of patches that reach the true vacuum and backreact during inflation, one must track the evolution of the fluctuations to $|h| \sim h_{s/r}$.

Before meaningful conclusions can be drawn from the solution of the FP equation, we must first understand how true vacuum patches form and evolve in spacetime as inflation proceeds and eventually ends. In the next section, we investigate this question with full dynamical simulations, before returning to the solution of the FP equation and discussing the implications for inflation in the subsequent section.

III. HIGGS AND SPACETIME DYNAMICS

This section, which comprises the main part of the paper, presents the results of general relativistic simulations to study the classical spacetime and field dynamics of Higgs fluctuations during inflation. In Sec. III A we outline our setup and methods for solving the field equations. We evaluate the time scale for a Higgs fluctuation to fall to the true vacuum in Sec. III B, and illustrate that the spatial extent of the field has a negligible effect on this in the relevant parts of parameter space. In Sec. III C we study the formation of a region of true vacuum. We find that the crunching region is hidden behind a black hole horizon, which is itself surrounded by an expanding region of negative energy density. In Sec. III D, we examine the growth of the regions rapidly evolving to the true Higgs vacuum, demonstrating that it is generically causally disconnected from the noninflating interior. As such, once formed, these regions expand and persist throughout inflation. Section III E is devoted to an examination of nonspherically symmetric Higgs fluctuations, illustrating how they can form arbitrarily elongated black holes and black strings by virtue of the negative potential energy of the Higgs field.

A. Numerical setup

To model the classical evolution of the Higgs field, we consider a scalar field h, with equation of motion $\Box h = V'$ (where, in terms of covariant derivatives, $\Box \equiv \nabla_a \nabla^a$), coupled to the Einstein field equations. For the purposes of the simulation, we add a Planck-suppressed operator to Eq. (2) to stabilize the potential at large field values,

$$V(h) = \Lambda_{\rm Infl} + \frac{\lambda}{4}h^4 + \frac{\lambda_6}{6M_P^2}h^6. \tag{5}$$

Here the constant term represents the contribution from the inflaton and is related to the Hubble scale during inflation as $\Lambda_{\rm Infl} = 3M_P^2H^2$, where M_P is the reduced Planck mass. The parameters $\lambda < 0$ and $\lambda_6 > 0$ are constants representing, respectively, the effective quartic term in the instability regime and some unknown higher-dimensional correction. The higher-dimensional correction generates a Planck-scale global minimum at

$$\frac{h_{\rm min}}{M_P} = 0.1\left(\frac{\lambda}{-0.01}\right)^{1/2}(\lambda_6)^{-1/2} \tag{6}$$

with value

$$\frac{V_{\rm min}}{\Lambda_{\rm Infl}} = 1 - 1.85\times 10^5\left(\frac{\lambda}{-0.01}\right) \times \left(\frac{\Lambda_{\rm Infl}}{(10^{16}\ {\rm GeV})^4}\right)^{-1}\left(\frac{h_{\rm min}}{0.1M_P}\right)^4. \tag{7}$$

For $h_{\rm min} \sim M_P$, $-V_{\rm min} \gg \Lambda_{\rm Infl}$. However, depending on the energy scale of inflation, the magnitude of the higher-order coupling, and the exact value of λ within the experimental error bars, it is conceivable that $h_{\rm min} \ll M_P$ or $h_{\rm min} \sim M_P$, as well as that $-V_{\rm min} \gg \Lambda_{\rm Infl}$ or $-V_{\rm min} \sim \Lambda_{\rm Infl}$. Keeping to cases with a negative energy density true vacuum with $V_{\rm min} \leq -\Lambda_{\rm Infl}$, we have considered all hierarchies and found that our main results do not depend strongly on the values of these parameters.[5] Hence, for presenting our results, we mainly choose the values of these parameters

[5]Note that the case where the true vacuum energy density does not exceed the inflationary energy density assumedly constitutes a worst-case scenario in which regions that transition to the true vacuum continue to inflate. So, such regions certainly persist throughout inflation, allowing them to nucleate and destroy any remaining space in the EW vacuum afterwards.

based on computational expediency without worrying about covering the entire physically viable parameter space; below we will use the default parameters $h_{\rm min} = 0.1M_P$ and $V_{\rm min}/\Lambda_{\rm Infl} = -100$ unless otherwise stated.

For initial conditions, we consider Higgs fluctuations that are momentarily static, $\partial_t h = 0$, and have axisymmetric spatial profiles. We consider both Gaussian spatial profiles given by

$$h(x,y,z) = h_{\rm in} e^{-\rho^2/2}, \quad \rho^2 = \frac{(x^2+y^2)}{R_{xy}^2} + \frac{z^2}{R_z^2}, \tag{8}$$

as well as, for illustrative purposes, compactly supported, step-function-like profiles given by

$$h = \begin{cases} h_{\rm in} & \text{if } \rho < 0.9 \\ 0 & \text{if } \rho \geq 1, \end{cases} \tag{9}$$

where the function smoothly interpolates in the range $0.9 \leq \rho < 1.0$. We mainly concentrate on the spherically symmetric case with $R_{xy} = R_z \equiv R$, but address nonspherical cases in Sec. III E. In presenting our results, we will make use of the coordinate radius $r_p = \sqrt{x^2+y^2+z^2}$, which will closely match standard planar dS coordinates for regions where there has not been a strong backreaction on the spacetime—i.e., a factor of e^{Ht} should be applied to obtain the proper radius.

During the evolution, we search for and, in many cases, find marginally outer trapped surfaces—apparent horizons—which signal the presence of black holes. In such cases, we excise the causally disconnected interiors of these surfaces from the numerical domain in order to continue the evolution outside the black holes. Further details of the implementation of the Einstein equations in our numerical simulations are described in the Appendix.

B. Time scale to fall to the true vacuum

First, we examine the time scale for the field to fall into the true vacuum. Given an initial unstable fluctuation in the Higgs field, both gradient spreading and Hubble friction counter this process. Taking a spherically symmetric Gaussian profile with radius R, the value where the spatial Laplacian term and the gradient of the potential term are equal and opposite at the maximum of the fluctuation is

$$h_c = -V'(h_c)\frac{R^2}{3}. \tag{10}$$

Hence fluctuations with $h_{\rm in} \gtrsim h_c$ for a given R will directly fall to the true vacuum, while those with $h_{\rm in} \lesssim h_c$ will only fall to the true vacuum after the exponential expansion increases their characteristic size, diluting the effects of spatial gradient terms.

Estimating the value below which Hubble friction prevents the field from falling to the true vacuum within roughly a Hubble time (i.e., for the field to exit the slow-roll regime) gives a similar value of h_c as in Eq. (10), but with $R = R_H \equiv H^{-1}$ [Eq. (4)]. Consequently, we expect fluctuations that have grown beyond h_c and $h_{s/r}$ to fall swiftly to the true vacuum. For smaller values, the evolution to the true vacuum takes several Hubble times or more, during which the fluctuation becomes exponentially larger in spatial extent due to inflation.

These expectations are corroborated by the simulations and illustrated in Fig. 1, where we plot the evolution of the maximum value of $|h(r)|$ for initial Higgs fluctuations of various sizes and magnitudes. Initial magnitudes larger than $h_{s/r}$ are found to fall rapidly into the true vacuum within $\sim$1 e-fold, and this behavior is largely insensitive to the exact initial size of the fluctuation—in the plot, the curves of $R/R_H = 1.0$, 4.0, and ∞ are very close together.

For spatially smaller fluctuations, the gradient terms and Hubble friction can significantly slow down this process (lowest blue, red, and green lines) and, in the extreme scenario of $R/R_H = 0.1$, can even be dominant enough to force the field back towards the EW vacuum even for $h > h_{s/r}$ (two lower black curves). However, the large Higgs fluctuations generated by inflation that are in danger of falling to the true vacuum are generated from superhorizon modes with $R > R_H$, which continue to inflate as they classically evolve to the true vacuum, resulting in a

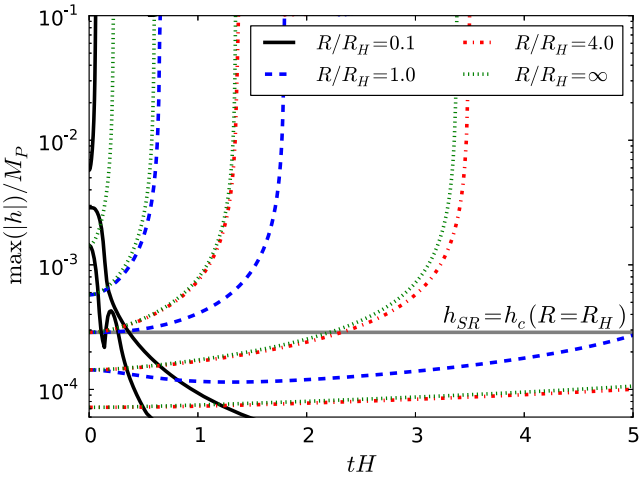

FIG. 1. Evolution of the maximum Higgs field value for initially spatially Gaussian fluctuations with size $R/R_H = 0.1$, 1.0, and 4.0 and various initial magnitudes. For comparison we also show the evolution of the amplitude when the initial radius is infinite (i.e., in an Friedmann-Robertson-Walker cosmology, with $R/R_H = \infty$; green dotted lines). The horizontal grey line indicates the approximate value where the field exits the slow-roll regime, which is also the approximate magnitude below which gradient spreading is important for $R = R_H$. The features in the lowest black curve are due to the shifting location of the maximum field value in this case.

characteristic size $R \gg R_H$. Hence we can safely assume that spatial variations have a negligible effect on the time for the development of a region of true vacuum for all realistic scenarios of interest.

C. Regions of true vacuum and formation of black holes

Regions where the Higgs field fluctuations fall towards the true vacuum experience a strong backreaction of the Higgs field on the spacetime. This terminates inflation locally in these regions and, as the energy density becomes negative, exponential expansion turns to contraction with the formation of a crunching region. Here we examine the details of this process.

In Fig. 2 we show the evolution of an example case where this occurs (similar results are found for other parameters). In addition to the value of the Higgs field, we also plot the energy density $\rho = n_a n_b T^{ab}$, a local measure of the Hubble expansion rate $\mathcal{H} \equiv \nabla_a n^a/3$, and a local measure of the number of e-folds of expansion $\mathcal{N}$ (found by integrating $n^a \nabla_a \mathcal{N} = \mathcal{H}$). These quantities are defined in terms of n^a, the unit normal to slices of constant coordinate time.

Previous studies have ignored the dynamics of the Higgs field in this process; we find, however, that they are crucial to understanding the evolution of the system. The Higgs fields falls towards the true vacuum, eventually oscillating around the global minimum (top-left panel of Fig. 2), with a large amount of the potential energy liberated by the field going into kinetic/gradient energy. The energy density at the center of the fluctuation grows (top-right panel) as this region contracts (bottom-left panel), leading to the formation of a black hole, as indicated by the presence of an apparent horizon inside the AdS-like region (denoted by dashed black lines in Fig. 2). The positive mass of the black hole is compensated by a shell of negative potential energy surrounding it (see the narrow blue strip adjacent to the black hole horizon in the top right panel); both increase in size as evolution progresses, with more and more of the energy obtained by the Higgs field falling to its true vacuum being locked behind the black hole horizon.

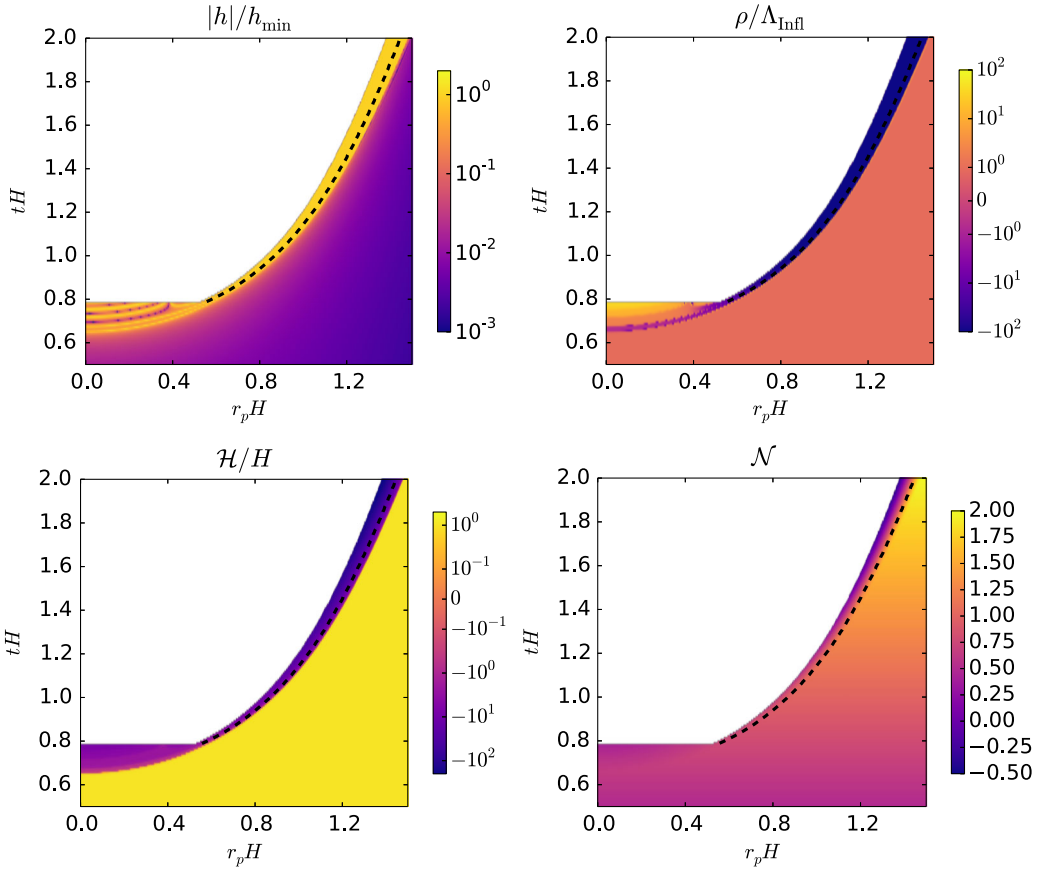

FIG. 2. An unstable Higgs field fluctuation falling to the true vacuum. We show, left to right, top to bottom: the Higgs field value, energy density, local Hubble expansion rate ($\mathcal{H} = -3K$) and local number of e-folds of expansion as a function of radius (in planar coordinates, r_p) and time. Results correspond to an initially spatially Gaussian fluctuation with $R = R_H$ and $h_{\rm in} = 2h_c$, and potential with $V_{\rm min}/\Lambda_{\rm Infl} = -100$ and $h_{\rm min}/M_P = 0.1$. The dotted black line indicates the surface of the apparent horizon that forms during the evolution, while the white space indicates the region behind the apparent horizon that is excised from the domain in order to continue the simulation.

This black hole hides any crunching singularity (potentially indicated by the negative values in the bottom-right panel) from outside observers. Note that the white space in the plots indicates regions inside the apparent horizon that are excised in order to continue the simulations. Though (as seen in the top-left panel of Fig. 2) the spatial region over which the Higgs field transitions from near the true vacuum to a much smaller value is small, as we detail below, the dynamics of the spreading of the fluctuation is not determined by the boundary of the region which has reached the true vacuum, and is thus qualitatively different from the thin-wall approximation where all the evolution is set by this interface.

D. Dynamics of bubble wall: Causally disconnected evolution

Next, we study how the fluctuation propagates outwards in spacetime. During inflation, an unstable Higgs fluctuation will both spread due to dispersion, as well as expand due to inflation, in spite of the eventual formation of a crunching region in the interior. The inflationary expansion is more important when the characteristic size of the fluctuation is greater than the Hubble radius, and occurs while the amplitude of the fluctuation increases as it falls to the true vacuum.

For this purpose, two different length scales are of interest: (i) the radius of the unstable Higgs fluctuation (i.e., the region that will rapidly diverge to the true vacuum), defined to be the outermost radius at which the field value is half the amplitude of the initial fluctuation, $h = \frac{1}{2}h_{\rm in}$, and (ii) the radius of the bubble of true vacuum (i.e., the region that has effectively reached the global minimum), defined to be the outermost radius where $h = \frac{1}{2}h_{\rm min}$. To illustrate the evolution of an unstable Higgs fluctuation and expanding bubble of true vacuum, in Fig. 3 (left panel) we plot how these two length scales grow as a function of time for a compactly supported Higgs fluctuation [given by Eq. (9)]. We plot these for both a Hubble radius-sized fluctuation and the limiting case of Minkowski space. As expected, in all cases the fluctuation radius increases ahead of the interior expanding bubble of true vacuum. While the comoving spread of the fluctuation will be slowed down by Hubble friction in the inflating case relative to Minkowski, its volume will also increase exponentially due to expansion.

The more interesting information is plotted in the second panel of Fig. 3, which shows the ratio of the change in proper length squared versus time squared $ds^2/dt^2 = g_{ab}(dr^a/dt)(dr^b/dt)$, where r^a is the spacetime coordinate of the fluctuation or bubble radius. While the edge of the Higgs fluctuation is moving outward at nearly the speed of light (i.e., $ds^2/dt^2 \sim 0$), the growth of the radius of the bubble of true vacuum is spacelike, $ds^2/dt^2 > 0$. This means that one should *not* view the bubble of true vacuum as causally sweeping outwards, converting dS into AdS. Rather, the correct interpretation is that after the unstable Higgs fluctuation (at the lower amplitude $\frac{1}{2}h_{\rm in}$ for which it does not backreact on the spacetime) reaches a given point, that point falls to the true vacuum causally disconnected from the fact that its neighboring points are also falling to the true vacuum. In the Minkowski limit, the spacetime curves traced out by the Higgs fluctuation and the bubble of true vacuum (blue lines) both approach being null. However, in de Sitter space, the exponential expansion eventually dominates, and the edge of the Higgs fluctuation quickly becomes causally disconnected from the bubble of true vacuum. This implies that the growth of the true vacuum region is insensitive to the behavior of the

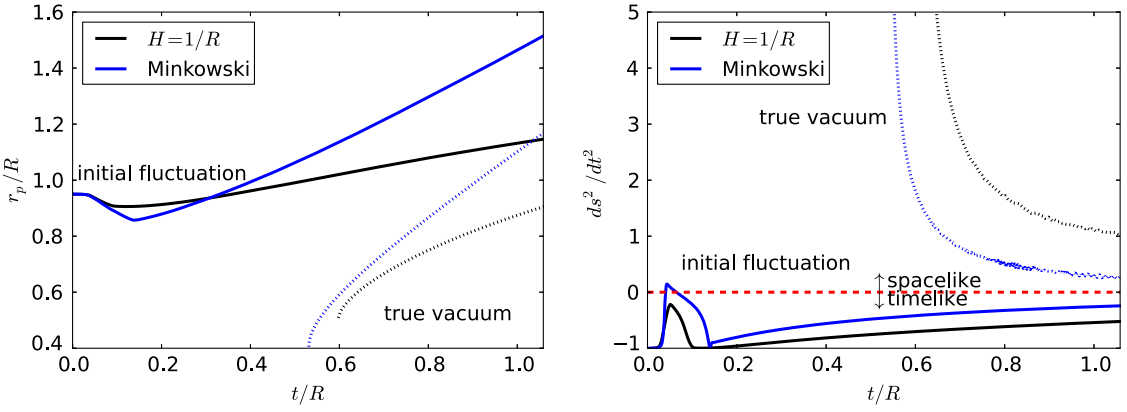

FIG. 3. Evolution of the size of a large Higgs fluctuation and resulting region of true vacuum in de Sitter (black lines) and Minkowski (blue lines) space. The left panel shows the outermost radius in planar coordinates [hence a factor of $\exp(tH)$ should be applied to obtain the proper radius], where the Higgs field equals $h_{\rm in}/2$ (roughly the radius of initial fluctuation; solid lines) and where the Higgs field equals $h_{\rm min}/2$ (roughly the radius of the true vacuum patch; dotted lines), as a function of time. The right panel shows proper length squared per time squared ds^2/dt^2 of these curves. The potential has $V_{\rm min}R^2/3 = 100$ and $h_{\rm min} = 0.1$. The initial fluctuation has a compactly supported spatial profile given by Eq. (9) (the transient behavior at early times being an artifact of this particular choice).

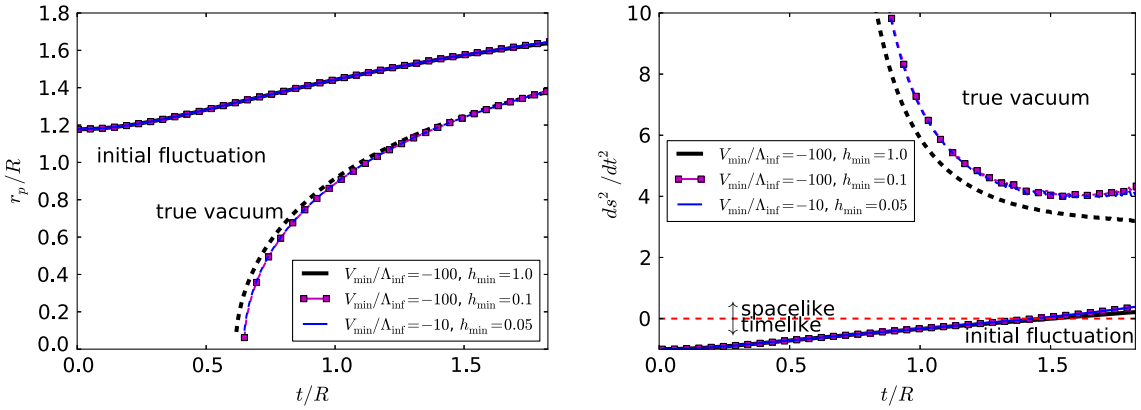

FIG. 4. Similar to Fig. 3, but for initially spatially Gaussian fluctuations in de Sitter with $R = R_H$. The three different cases shown have $(V_{\rm min}/\Lambda_{\rm Infl}, h_{\rm min}/M_P) = (-100, 1.0)$ (black), $(-100, 0.1)$ (red), and $(-10, 0.05)$ (blue), but show similar behavior.

spacetime in the interior region and the details of the Higgs potential near $h_{\rm min}$. The Minkowski result also illustrates that the true vacuum regions will continue to grow after the end of inflation when the surrounding energy density is reduced.

Similar results are also obtained for spatially Gaussian fluctuations, which we show in Fig. 4. It should be noted that the location of the boundary of the fluctuation is less well defined in this case (and the boundary region is also being expanded out of casual contact as seen in the left panel at late times). This plot demonstrates that the exact parameters of the Higgs potential near its minimum make little difference to the growth. Finally, we note that while a region of true vacuum can become exponentially large during the de Sitter phase, it of course cannot extend past the cosmological horizon of the initial Higgs fluctuation that gave rise to it. So, the creation of a single unstable fluctuation cannot globally terminate inflation. However, this may occur if a sufficient proportion of the space transitions to a crunching phase [35], perhaps implying constraints on any phase of inflation occurring before that giving rise to our observable Universe.

E. Beyond spherical symmetry: Black holes and violation of hoop conjecture

So far, we have focused on spherically symmetric configurations. However, the assumption of spherical symmetry strongly limits the spacetime dynamics (for example precluding the existence of gravitational waves) and hence the range of solutions uncovered by our simulations. Furthermore, since a large Higgs fluctuation that has become classical arises from the stochastic addition of many modes, there is no reason to expect it to be spherical, so that it is important to study this broader class of fluctuations. For these reasons, we now extend our studies to nonspherically symmetric (though still axisymmetric) cases.

We find that such configurations evolve similarly in many ways to the spherically symmetric cases considered above. In Fig. 5, we show results from a case identical to the one shown in Fig. 2, except with $R_z = 2R_{xy} = R_H$ instead of $R_{xy} = R_z = R_H$. In both cases, the field swiftly falls to the true vacuum, creates a crunching region, and forms an apparent horizon. Thus our observations from the previous subsections also apply to nonspherical configurations.

More interestingly, we find that there are significant differences between the large Higgs fluctuation cases we study here—which produce regions of negative energy density—and spacetimes that satisfy standard energy conditions. In particular, for four-dimensional spacetimes with positive energy, black hole apparent horizons are found to always have spherical topology [36,37]. Furthermore, it has been found that, geometrically, black holes cannot be arbitrarily elongated. The latter condition is encapsulated in the hoop conjecture [29], which states that a region containing a mass M will form a black hole with attendant horizon if and only if a "hoop" of circumference $4\pi M$ can be passed over the region in every direction. For example, the collapse of an infinite cylinder will not form a horizon, but instead create a naked singularity. Crucially, these restrictions do not apply to AdS spacetimes, which can develop cylindrical black holes [38,39]. Analogously, we find that they also do not apply in our study of Higgs fluctuations because the regions in which the Higgs field diverges to the true vacuum evolve into regions with negative potential energy, allowing for the formation of arbitrarily elongated black holes.

To demonstrate this, we consider a series of increasingly elongated Gaussian field configurations. We fix the radius in the equatorial plane, $R_{xy} = R_H$, and consider cases with larger and larger extent along the symmetry axis, $R_z/R_{xy} = 1$, 2, 4, and 8. In all cases we find that an apparent horizon does form soon after the Higgs fluctuation reaches the true vacuum. As shown in Fig. 6, the proper equatorial circumference C_{eq} of the horizon evolves in a similar manner for all cases, indicating that the narrow "waist" of the Higgs fluctuation and resulting black hole is

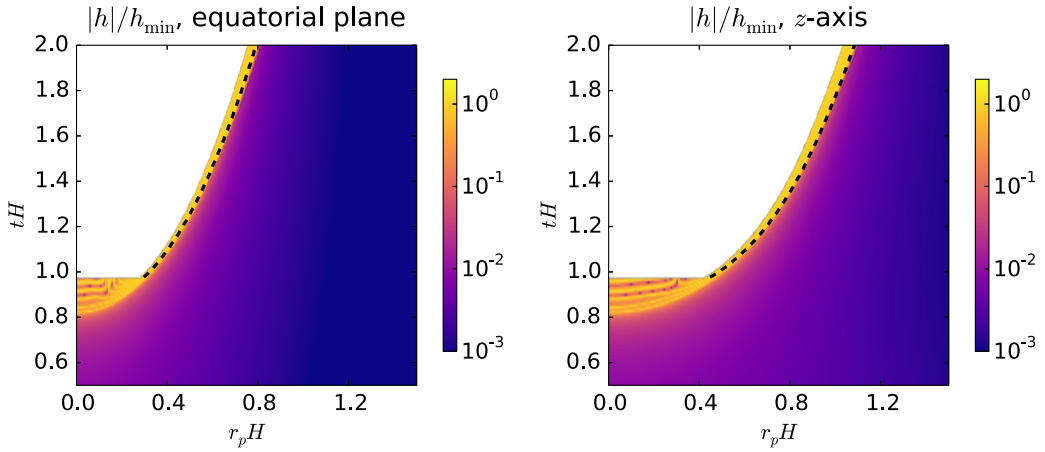

FIG. 5. The Higgs field fluctuations as a function of radius (in planar coordinates, r_p) and time for the evolution of an initial fluctuation that is an elliptical Gaussian with $R_z = 2R_{xy} = R_H$. The left panel shows the field in the equatorial plane, while the right panel shows the field on the symmetry axis. Except for the absence of spherical symmetry, the parameters in this case are the same as the ones shown in Fig. 2, and the evolution proceeds in a similar manner.

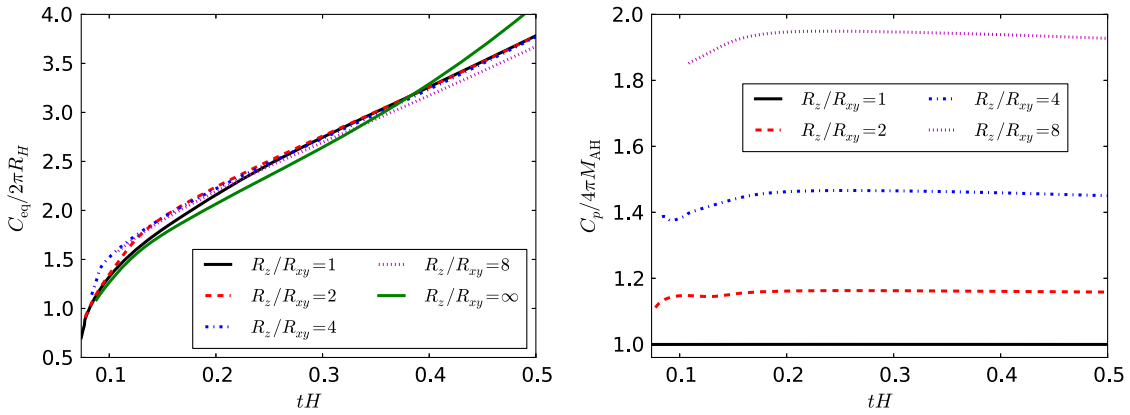

FIG. 6. The proper equatorial (left panel) and poloidal (right panel) circumferences of the apparent horizons that form from large Higgs field fluctuations (beginning from when they are first found in the domain) with various aspect ratios R_z/R_{xy}. We also show the equatorial circumference of a case with z-translational symmetry ($R_z/R_{xy} = \infty$) where the horizon has cylindrical topology. The poloidal circumference is normalized by the horizon mass M_{AH} to show how far above the hoop conjecture criterion $C \lesssim 4\pi M_{\rm AH}$ it is in each case.

not sensitive to the longer direction. The poloidal circumference C_p does, however, increase with the increasing aspect ratio, and it increases at a greater rate than the mass of the horizon $M_{\rm AH}$ (measured from its proper area), giving larger and larger violations of the hoop conjecture criterion.

Although configurations with larger aspect ratios become increasingly difficult to track numerically, we can also consider the infinite R_z/R_{xy} case by evolving a spacetime with an enforced translational symmetry in the z-direction.[6] We find that a horizon also forms in this case, now with *cylindrical* topology, i.e., a black string. From Fig. 6 we can see that the evolution of its circumference proceeds in a similar manner to the other cases. These results suggest that, even proceeding from a slice of $3+1$ dimensional (very nearly) de Sitter spacetime, the presence of a Higgs field potential with a negative minimum enables the formation of arbitrarily elongated, stringlike horizons. Thus the hoop conjecture is violated in favor of ensuring that cosmic censorship—the requirement that singular regions be hidden from outside observers—is obeyed.

IV. NUMERICAL SOLUTIONS OF THE FOKKER-PLANCK EQUATION AND IMPLICATIONS FOR COSMOLOGICAL HISTORY

In the previous section, we established with solutions in full General Relativity that, for reasonable parameters,

[6]For this one case, we use periodic boundary conditions in the x and y directions, though with the boundary at large enough distances so as to be insignificant to the results shown here.

regions of space exhibiting sufficiently large Higgs fluctuations $|h| \gtrsim h_{s/r}$ do rapidly fall to the true vacuum and create persistent crunching regions, both in an inflating spacetime, and in the limiting case of an approximately Minkowski spacetime. The formation of any such fluctuation during inflation would therefore be fatal for our Universe, as it would expand after inflation has ended, destroying the surrounding (approximately) Minkowski space in the EW vacuum. Having established this result, we now return to the stochastic approach, introduced in Sec. II, to determine the implications for the scale of inflation. In contrast to previous work that also solved the FP equation, here we numerically resolve the exponentially suppressed tails of the distribution, which, as we will show, impacts the constraint on $H/\Lambda_{\max}$. Below, in Sec. IV A, we compare the exact solution to previous approximations.

We are interested in solving the FP equation to determine when at least one true vacuum patch has formed in our past light cone, i.e.,

$$P(|h| \gtrsim h_{s/r}, N) e^{3N} \geq 1 \tag{11}$$

after N e-folds of inflation. We rewrite the FP equation [Eq. (1)] in terms of the variable $X \equiv \log P$,

$$\frac{\partial X}{\partial t} = \frac{V''(h)}{3H} + \frac{V'(h)}{3H}\frac{\partial X}{\partial h} + \frac{H^3}{8\pi^2}\left[\frac{\partial^2 X}{\partial h^2} + \left(\frac{\partial X}{\partial h}\right)^2\right], \tag{12}$$

and numerically solve for X. This is essential for resolving the exponentially small tails of the distribution that determine probabilities, of order e^{-3N}, for obtaining $|h| \gtrsim h_{s/r}$. Given X, one can calculate, for instance, the maximum number of e-folds $N_{\max}$ that inflation can proceed without the formation of a true vacuum patch, i.e., without Eq. (11) being satisfied. Note that, as stressed in [24], integrated "transition probabilities" to find the Higgs field beyond a certain value, such as $P(|h| \gtrsim h_{s/r}, N)$ in Eq. (11), are gauge invariant. However, for simplicity and to allow comparison to prior results, we will frequently quote results in terms of $\Lambda_{\max}$ (or rather $H/\Lambda_{\max}$) computed in Landau gauge.

As we are interested in the formation of a true vacuum patch only in our past light cone, we need only consider the ensemble of patches arising from the progenitor patch that inflated $N \simeq 50$–60 e-folds before the end of inflation to give rise to our observable Universe [40]. We (optimistically) assume this patch began the relevant period of inflation in the electroweak vacuum, i.e., with $P(h, 0) \simeq \delta(h)$. More details on solving the FP equation, including the exact initial conditions used, are given in the Appendix.

We calculate the appropriate Higgs quartic for Eq. (2) using two-loop renormalization-group improved couplings and including one-loop contributions to the effective potential [41], specifically

$$V_{\text{eff}} = \frac{\lambda(\mu) + \lambda^{(1)}_{\text{eff}}(\mu \simeq \sqrt{h^2 + H^2})}{4} h^4, \tag{13}$$

where the one-loop contribution to the quartic is

$$\begin{aligned}\lambda^{(1)}_{\text{eff}}&(\mu \simeq \sqrt{h^2 + H^2}))\\ &\simeq \frac{1}{16\pi^2}\left\{\frac{3g_2^2}{8}\left(\log\frac{g_2^2}{4} - \frac{5}{6}\right)\right.\\ &\quad + \frac{3(g_2^2 + g_Y^2)}{16}\left(\log\frac{g_2^2 + g_Y^2}{4} - \frac{5}{6}\right)\\ &\quad \left. - 3y_t^4\left(\log\frac{y_t^2}{2} - \frac{3}{2}\right)\right\}.\end{aligned} \tag{14}$$

We match observed quantities to $\overline{\text{MS}}$ parameters using expressions from [11]. In the parameter space of interest, we find that the scale at which the quartic is to be evaluated, $\mu \simeq \sqrt{H^2 + h^2}$, lies within approximately an order of magnitude of $\Lambda_{\max}$. As such, a suitable approximation for the running coupling is

$$V(h) \simeq -b_0 \log\left(\frac{H^2 + h^2}{\sqrt{e}\Lambda_{\max}^2}\right)\frac{h^4}{4}. \tag{15}$$

Taking the central values for the Higgs mass $m_h = 125.09 \pm 0.24$ GeV [42] and the top quark mass $m_t = 172.44 \pm 0.70$ GeV [43], we find $b_0 \simeq \frac{0.12}{(4\pi)^2}$ and $\Lambda_{\max} \simeq 3.0 \times 10^{11}$ GeV.[7] The corresponding values of h_{cl}, $h_{s/r}$ depend somewhat on H, but tend to be $h_{\text{cl}} \simeq 1.2\Lambda_{\max}$ and $h_{s/r} \simeq \text{few} \times \Lambda_{\max}$ in the parameter space of interest.

The dependence of $N_{\max}$ on $H/\Lambda_{\max}$ is shown in the left panel of Fig. 7 (solid, black). In particular, if we require that inflation lasts at least 60 e-folds, we find

$$\begin{aligned}&\frac{H}{\Lambda_{\max}} \lesssim 0.067 \Rightarrow \text{no true vacuum patches}\\ &\qquad (\text{i.e., with } |h| > h_{s/r}) \text{ form during inflation}\end{aligned} \tag{16}$$

for the central values of (m_h, m_t) quoted above.

We note that this limit is maximally conservative—for $H/\Lambda_{\max}$ satisfying Eq. (16), patches in which $|h| > \Lambda_{\max}$ may still be formed. These can in principle be stabilized by, e.g., efficient reheating [24], but this implies a condition on postinflationary cosmology. If reheating is not sufficiently efficient to drive these patches back to the electroweak

[7]Here, we use the recently updated measurement of m_t from CMS as it is subject to the smallest uncertainties, but note that ATLAS has also recently published a comparable measurement $m_t = 172.84 \pm 0.86$ GeV [44]. In addition to the experimental uncertainties, we have added in quadrature 0.5 GeV of theoretical uncertainty to account for conversion between a Monte Carlo and on-shell top mass definition [45,46].

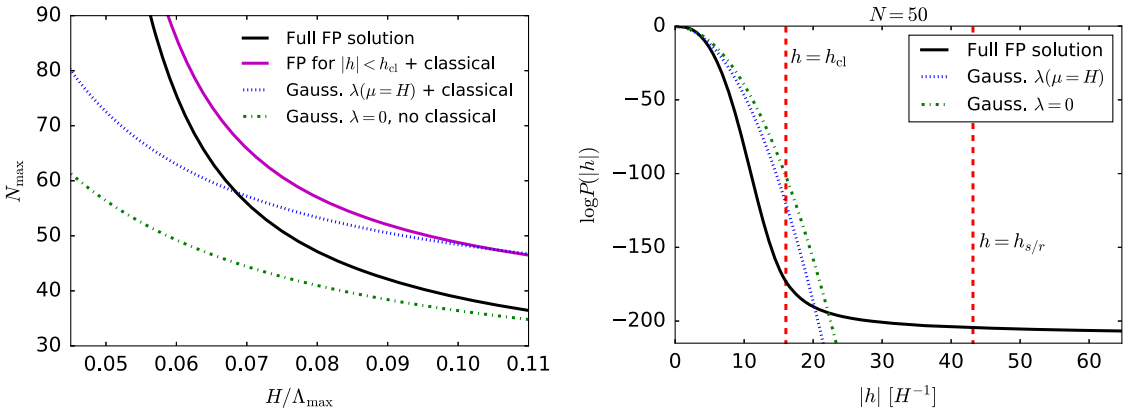

FIG. 7. Left panel: The maximum number of e-folds that inflation can proceed without the formation of a true vacuum patch $N_{\rm max}$ as a function of $H/\Lambda_{\rm max}$. Right panel: Probability distribution of the Higgs field after $N = 50$ e-folds for $H/\Lambda_{\rm max} = 0.067$. In both cases, the full FP treatment is compared to other approaches. Note the long, non-Gaussian tail that develops at high field values in the right panel due to (as discussed below) the strong effect of the negative quartic in this regime.

vacuum, they will ultimately classically evolve to the true vacuum, which would still prove disastrous for our Universe. Thus, we can also consider the more stringent requirement that no patches in our past light cone fluctuate beyond the maximum of the potential during inflation. In this case, we find

$$\frac{H}{\Lambda_{\rm max}} \lesssim 0.064 \Rightarrow \text{no patches with } |h| > \Lambda_{\rm max} \text{ form during inflation.} \quad (17)$$

These are our main results, and represent the most accurate constraints on H in the presence of a SM vacuum instability.

We present these results in the (m_h, m_t) plane in Fig. 8, taking the maximally conservative upper limit on the inflationary Hubble scale subject to the requirement $N_{\rm max} \geq 60$ (solid) or $N_{\rm max} \geq 50$ (dashed). The limit on $H/\Lambda_{\rm max}$ varies nontrivially with b_0, as can be seen in Fig. 9. For fixed $H/\Lambda_{\rm max}$, larger b_0 (corresponding to larger m_t for a given m_h) results in a more positive quartic at the scale $\mu \simeq H < \Lambda_{\rm max}$ relevant for small fluctuations, which produces a greater stabilizing effect. But, it also leads to more rapid growth of larger (superbarrier) fluctuations for which the quartic is more negative. As such, the variation in the limit depends on which effect dominates. Interestingly, the limit is approximately strongest for the value of b_0 favored by the central (m_h, m_t) values. However, this limit depends only weakly on b_0 throughout the SM parameter space, ranging between $0.06 \lesssim \frac{H}{\Lambda_{\rm max}} \lesssim 0.11$ for $\frac{0.01}{(4\pi)^2} \lesssim b_0 \lesssim \frac{0.40}{(4\pi)^2}$ and $N_{\rm max} = 60$. Hence, the bounds on H are mainly driven by how $\Lambda_{\rm max}$ varies with (m_h, m_t) and, for a given m_h, the rapid decrease in $\Lambda_{\rm max}$ with increasing m_t results in significantly more stringent limits on H.

The region in which the Higgs potential is stable up to the Planck scale is shown in green, while the region in blue corresponds to where the potential is unstable, but current limits on $r < 0.07$ [47] permit the Universe to exit inflation without producing a patch of true vacuum. We also highlight in red the parameter space where the vacuum instability would preclude $N_{\rm max} > 60$ for $r \gtrsim 0.002$. In other words, in the event of a near-future detection of

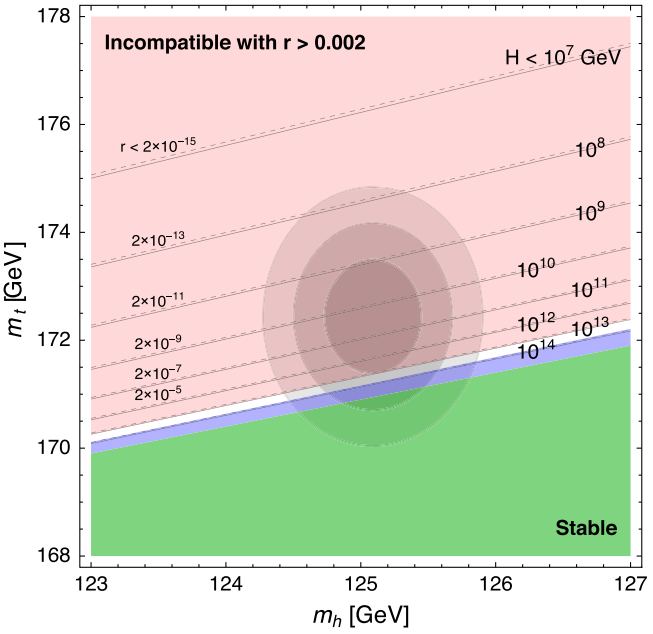

FIG. 8. Limits on H [GeV] (black contours) in the (m_h, m_t) plane requiring $N_{\rm max} \geq 60$ (solid) or 50 (dashed). Central values are taken to be $m_h = 125.09 \pm 0.24$ GeV [42] and $m_t = 172.44 \pm 0.70$ GeV [43], with contours corresponding to 1-, 2-, and 3-σ regions as for two parameters. The shaded regions represent: the Higgs potential is stable up to M_P (green); the Higgs potential is unstable, but current limits $r < 0.07$ [47] permit required amount of inflation (blue); and instability would preclude the combination of $N_{\rm max} > 60$ and $r > 0.002$, to be probed by near-future experiments [12] (red).

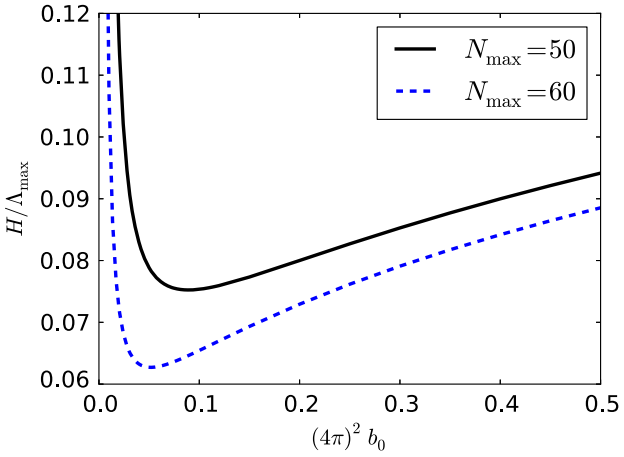

FIG. 9. The bounds on the ratio $H/\Lambda_{\max}$ as a function of b_0, the β function near the maximum of the potential [see Eq. (15)], requiring $N_{\max} = 50$ (black, solid) or $N_{\max} = 60$ (blue, dashed).

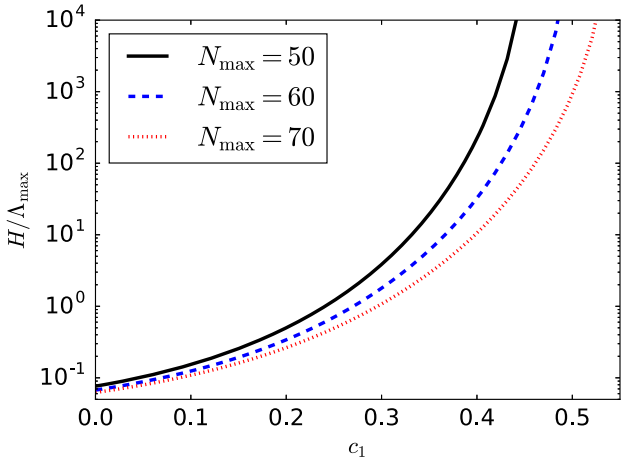

FIG. 10. The bounds on the ratio $H/\Lambda_{\max}$ when the term $\frac{1}{2}c_1H^2h^2$ is included in the Higgs potential, for $N_{\max} = 50$, 60, and 70 e-folds of inflation.

primordial B-modes, this region would require stabilizing corrections to the Higgs potential in order to exit inflation without producing a patch of true vacuum. It is notable that the lower central values for m_t favored by [43,44] (compared to the old global value $m_t = 173.34$ GeV [48]) increases the amount of parameter space known to be compatible with any possible inflationary scale. However, the best-fit values would still require $H \lesssim 10^{10}$ GeV ($r \lesssim 2 \times 10^{-9}$).

The limits given here are subject to some uncertainty, for instance resulting from the logarithmic running approximation employed in Eq. (15). In using a quartic potential, we also neglect any quadratic terms. At large field values, the effects of the Higgs mass-squared parameter are small, but we are also assuming that terms of the form H^2h^2 are suppressed as for a(n approximately) conformally coupled scalar. Note that, even in the absence of a direct Higgs coupling to curvature, Higgs couplings will radiatively generate H^2h^2 terms as in [19], but the loop-sized coefficients reduce the impact of such terms (see, e.g., Fig. 10). We return to the effect of such terms with more generic coefficients in Sec. IV B. There is also uncertainty due to the precise matching scale used for the quartic, as well as subdominant residual gauge variation as a result of the leading order approximations employed. While the exact error is difficult to quantify, we estimate it to be ∼10%, comparable to that resulting from the exact $N_{\max}$ required. As such, the variation in limits between $N_{\max} = 50$ and $N_{\max} = 60$ may be taken as approximately representing the uncertainty.

A. Comparison to approximate FP solutions

For the interested reader, we now compare our results to those obtained from employing various approximations, both in order to highlight several important effects captured by the full FP solution and to make connection with previous literature.

One approach, employed in several earlier works [13,17,23,24], is to approximate the field distribution as Gaussian,

$$P(h,N) = \frac{1}{\sqrt{2\pi\langle h^2\rangle}}\exp\left[-\frac{h^2}{2\langle h^2\rangle}\right], \tag{18}$$

in the quantum-dominated regime $|h| < h_{\rm cl}$. For a potential $V = \frac{\lambda h^4}{4}$ with constant λ, which we take to be $\lambda(\mu = H)$, the variance can be computed via the equation of motion [23]

$$\frac{d}{dt}\langle h^2(t)\rangle = \frac{2\lambda}{H}\langle h^2(t)\rangle^2 + \frac{H^3}{4\pi^2}. \tag{19}$$

The solution to this equation when $\lambda > 0$ is

$$\langle h^2(t)\rangle = \frac{1}{\sqrt{2\lambda}}\frac{H^2}{2\pi}\tanh\left(\sqrt{2\lambda}\frac{N}{2\pi}\right) \tag{20}$$

with tanh replaced by tan for $\lambda < 0$. For $\lambda \to 0$, this reproduces the result found in [17], and later in [24], for a negligible quartic coupling. The probability of finding a fluctuation $|h| \geq h_0$ is then given by

$$\begin{aligned} P(h \geq h_0, N) &= 1 - \mathrm{erf}\left(\frac{h_0}{\sqrt{2\langle h^2\rangle}}\right) \\ &\simeq \sqrt{\frac{2\langle h^2\rangle}{\pi h_0^2}}\exp\left(-\frac{h_0^2}{2\langle h^2\rangle}\right). \end{aligned} \tag{21}$$

Clearly, this approach does not accurately describe the behavior of large fluctuations. First, for $|h| \gtrsim H$, $\lambda(\mu \simeq \sqrt{H^2 + h^2}) \neq \lambda(\mu = H)$. This running of λ is

subdominant in the quantum-dominated regime $|h| \lesssim h_{\rm cl}$, but needs to be appropriately addressed for larger fluctuations $|h| \gtrsim h_{\rm cl}$, where classical evolution dominates. Second, previous implementations of this approach (such as Ref. [17] and later Ref. [24]), simply assumed that locally the field instantaneously evolves to the true vacuum once a fluctuation reaches $|h| \gtrsim h_{\rm cl}$. But, this does not appropriately account for the finite time taken for the fluctuation to diverge. Here, we attempt to account for this additional time by calculating how long it takes for a patch to evolve from $|h| \simeq h_{\rm cl}$ to $|h| \simeq h_{s/r}$ under the classical equation of motion,

$$\ddot{h} + 3H\dot{h} + V'(h) = 0, \tag{22}$$

which we denote $\Delta N_{\rm cl}$. As such, we estimate $N_{\rm max} \simeq N_{\rm cl} + \Delta N_{\rm cl}$.[8] Typically, $\Delta N_{\rm cl} \sim 10$–$20$.

In Fig. 7, we show $N_{\rm max}$ obtained using this prescription (left panel; blue, dotted), as well as from the similar prescription of Ref. [24] [Eq. (32) therein], which uses $\lambda = 0$ and neglects classical evolution (green, dash dotted). Comparing these results demonstrates the importance of both (i) the stabilizing effect of the quartic for small fluctuations (as $H < \Lambda_{\rm max}$) and (ii) the additional time taken for a true vacuum patch to form due to the duration of the classically dominated evolution. Together, these effects substantially extend the time taken for a true vacuum patch to form, relaxing the limit on H from $H/\Lambda_{\rm max} \lesssim 0.045$ as in [24] [or $H/\Lambda_{\rm max} \lesssim 0.046$ for the central (m_h, m_t) used here] to $H/\Lambda_{\rm max} \lesssim 0.065$.

However, this procedure underestimates the effect of the quartic in both regimes. For small fluctuations in the quantum-dominated regime, the Gaussian approximation underestimates the stabilizing impact. This can be seen in the right panel of Fig. 7, which compares the full FP solution to Gaussian approximations—for the full solution, the distribution is concentrated at smaller $|h|$. By itself, this would further enhance the time taken for a true vacuum patch to form; for instance, the magenta solid line of Fig. 7 employs the same procedure for matching between quantum- and classical-dominated phases as for the Gaussian approximations, but uses the full FP solution for $|h| \leq h_{\rm cl}$. This gives the less stringent limit $H/\Lambda_{\rm max} \lesssim 0.076$. However, that this limit is even weaker than the actual limit obtained from the full FP solution, Eq. (16), reveals that the quartic also accelerates the growth of large fluctuations relative to the classical expectation, resulting in elongated, non-Gaussian tails of $P(h,t)$ at large fluctuations (the importance of which was first emphasized in [23]). These tails are also visible in the right panel of Fig. 7 and mean that, by the time we expect a patch with $|h| > h_{\rm cl}$ to have formed, this patch is not so overwhelmingly likely to have $|h| \simeq h_{\rm cl}$ as opposed to some larger value (which would take less time to diverge to the true vacuum). As such, it does not take the full $\Delta N_{\rm cl}$ e-folds for a true vacuum patch to form, so the actual limit is slightly more stringent than $H/\Lambda_{\rm max} \lesssim 0.076$. Likewise, the slow falloff of the non-Gaussian tails of the distribution in the range $|h| > \Lambda_{\rm max}$, coupled with the exponentially increased volume from inflation, is the source of the similarity between Eqs. (16) and (17).

As a final point of comparison, we note that a Hawking-Moss (HM) calculation gives the probability for the Higgs field in a Hubble patch to transition to the top of the potential barrier,

$$P_{\rm HM} \simeq \exp\left[-\frac{8\pi^2 V(\Lambda_{\rm max})}{3H^4}\right]. \tag{23}$$

Requiring that no patches transition out of the EW vacuum via a HM instanton within $N_{\rm max} = 60$ e-folds of inflation gives the limit $H/\Lambda_{\rm max} \lesssim 0.061$, in good agreement with Eq. (17). This provides a useful consistency check, since the FP approach should reproduce the HM transition probability in the $H \ll \Lambda_{\rm max}$ regime [17].

Overall, we find that, in the presence of a Higgs vacuum instability, the existence of our Universe requires that any inflationary epoch satisfy $H \lesssim 0.07\Lambda_{\rm max}$. Moreover, we note that this result is fairly insensitive to postinflationary physics; while the constraint does weaken if we suppose fluctuations beyond the barrier are stabilized by, e.g., efficient reheating, the long, non-Gaussian tails of the fluctuation probability distribution make this effect small.[9]

B. Effect of stabilizing correction to the Higgs potential

Finally, we comment on the possibility of additional Higgs couplings to inflationary dynamics that may be capable of sufficiently stabilizing the Higgs potential during inflation. For instance, Higgs-inflaton and Higgs-curvature couplings are generally induced by loop corrections [19,49] and have been suggested as a minimal stabilization mechanism [13,14,17–19,24,50] of the EW vacuum during inflation because of their contribution to the effective mass of the Higgs. Similarly, Planck-suppressed operators coupling the Higgs to the inflaton or the inflaton potential can result in a large effective mass [17], e.g.,

[8] For a Gaussian distribution, this is a reasonable approximation because the bulk of the distribution with $|h| \gtrsim h_{\rm cl}$ is concentrated near $|h| \simeq h_{\rm cl}$ (larger fluctuations being exponentially less likely). Thus, the time taken for the part of the distribution with $|h| \gtrsim h_{\rm cl}$ to spread to $|h| \gtrsim h_{s/r}$ should be approximately given by $\Delta N_{\rm cl}$.

[9] Points at the tail of the distribution exit the slow-roll regime, and diverge rapidly to the true vacuum and backreact on spacetime *within a single Hubble time*; it is unlikely that any restoring preheating/reheating dynamics, however extreme, can come into full effect on such short time scales.

$$V \supset \frac{kV_I h^2}{M_P^2} = 3kH^2h^2, \tag{24}$$

which for $k > 0$ would stabilize the vacuum at $h = 0$.[10]

Using the methods outlined above, we can determine the importance of such additional terms in the Higgs potential for delaying the development of a patch of true vacuum. We will simply consider adding a term of the form

$$V \supset \frac{c_1}{2}H^2h^2 \tag{25}$$

to Eq. (15) during inflation and remain agnostic to the source of such a term—though, as we comment below, the underlying interaction responsible for generating this term may have important implications.

In Fig. 10, we show how the constraint on $H/\Lambda_{\max}$ is relaxed for various values of the coefficient c_1. For $c_1 \sim 1/4$, the bound on the energy scale of inflation is weakened to $H \lesssim \Lambda_{\max}$ while, for sufficiently large values of $c_1 \gtrsim 1/2$, the EW vacuum becomes effectively stable throughout inflation, such that any value of H is permissible (as anticipated from the HM calculation of [17]). This is because the typical size of fluctuations goes as $\sim \frac{H}{2\pi}\sqrt{N}$ while the additional term stabilizes the potential up to $h \sim \sqrt{\frac{c_1}{|\lambda|}}H$. Since the asymptotic value of $|\lambda|$ is small for the SM Higgs ($|\lambda| \lesssim 0.01$), even a modest coefficient c_1 can result in a rapidly weakening constraint on $H/\Lambda_{\max}$. Note that here, as $\mu \simeq \sqrt{H^2 + h^2}$ varies over a number of orders of magnitude, the logarithmic approximation employed in Eq. (15) is no longer valid. Therefore to obtain these results, we use the full running coupling. A negative value of c_1 would of course have the opposite effect, destabilizing the Higgs potential.

It is worth noting that, depending on the source of this coupling, the coefficient c_1 cannot be arbitrarily large, as such couplings may destabilize the Higgs field after inflation [52,53]. Specifically, after inflation, the Universe typically undergoes a period of preheating, during which the inflaton oscillates with large amplitude. These oscillations can induce large Higgs fluctuations via parametric resonance through the same coupling c_1 responsible for stabilizing the Higgs during inflation. Sufficiently large fluctuations would generate a negative effective Higgs mass and tachyonic instability, triggering EW vacuum decay, and this implies an upper bound on c_1 [54,55]. For instance, supposing that the Higgs couples to the inflaton ϕ as $V \supset \frac{c_1^2}{2}\phi^2h^2$ and that the inflaton oscillates with chaotic inflationlike parameters ($m_\phi \simeq 10^{13}$ GeV and initial amplitude $\phi_0 \simeq M_P$), the analysis of [54] would constrain $c \lesssim 10^{-4}$ or $c_1 \lesssim \mathcal{O}(10^3)$.

While this is an important constraint, it is clear that, if the Higgs-inflaton coupling were to arise from an operator like Eq. (24), such large values would require that this operator was generated with a significantly larger coefficient than the $\mathcal{O}(1)$ value expected in effective field theory, or that the cutoff was somewhat below the Planck scale. In addition, the full details of the preheating and reheating phases are complicated. Notably, interactions of the Higgs field with SM particles produced via perturbative or nonperturbative Higgs decays [16,56–59] would result in finite density (or thermal) corrections that tend to stabilize the Higgs effective potential. As such, efficient thermalization may relax the bounds or even prevent EW vacuum decay during preheating. While these effects were estimated in [54], further dedicated numerical studies may be required to determine the exact bounds on Higgs-curvature or Higgs-inflaton couplings.

V. CONCLUSIONS

We have studied the dynamical response of inflating spacetime to unstable fluctuations in the Higgs field with numerical simulations of Einstein gravity. Our results offer, for the first time, an in-depth understanding of how spacetime evolves as a Higgs fluctuation falls towards, and eventually reaches, the true, negative energy, vacuum. We find that when true vacuum patches stop inflating and create a crunching region, and the energy liberated creates a black hole surrounded by a shell of negative energy density. This region of true vacuum persists and grows throughout inflation, with more and more energy being locked behind the black hole horizon. In contrast to the naive expectation that this growth is due to the boundary between true and metastable vacua sweeping outward in space, in an exponentially expanding spacetime the growth occurs in a causally disconnected manner. Spatial points fall to the true vacuum independent of the fact that neighboring points have also reached the true vacuum. Hence, under most circumstances, this process is insensitive to the behavior in the interior region, and to the exact shape of the potential close to the true minimum.

We also explored nonspherically symmetric solutions, where, in addition to confirming that the results from the spherically symmetric case apply more generally, we found that the formation of black holes with arbitrarily elongated horizons, or even black strings, was possible, in violation of the hoop conjecture. As such, the Higgs instability provides a quite different setting—one proceeding from an initially dS-like spacetime—where some of the exotic features seen in AdS-like spacetimes are realized.

We also extended the numerical solution of the Fokker-Planck equation to resolve the field distribution in the exponentially suppressed tails. This is necessary to extract the tiny probabilities associated with a single true vacuum patch in our past light cone, while simultaneously

[10]A related alternative is that Higgs couplings to moduli may modify and stabilize the potential as in, e.g., [51]. Here we focus on couplings directly to H.

incorporating the effects from renormalization group running of the quartic in the Higgs potential on the evolution of the probability distribution. Using this solution, in conjunction with the result from our classical General Relativity simulations that a single true vacuum patch in our past light cone destroys the Universe, we derived a bound $H/\Lambda_{\rm max} \lesssim 0.07$ on the scale of inflation. This bound is the most accurate available to date, and we compared it to bounds derived previously. We also found, as shown in Fig. 8, that a future measurement of the tensor to scalar ratio with $r > 0.002$ would imply the need for a stabilizing correction to the Higgs potential at a scale $\lesssim 10^{14}$ GeV supposing $m_t \gtrsim 171.4$ GeV. We are thus able to correlate a cosmological quantity with the necessity of stabilizing corrections to the Higgs potential.

Finally, we reemphasize that the results in this paper are of wider interest than the SM Higgs potential, as they are applicable to the inflationary dynamics of any scalar field with a negative energy true vacuum.

ACKNOWLEDGMENTS

We thank the Universe for surviving. J. K. also thanks Andrew Long for helpful discussions. Simulations were run on the Sherlock Cluster at Stanford University. This research was supported in part by Perimeter Institute for Theoretical Physics. Research at Perimeter Institute is supported by the Government of Canada through the Department of Innovation, Science and Economic Development Canada and by the Province of Ontario through the Ministry of Research, Innovation and Science. J. K. is supported by the DOE under Contract No. DE-SC0007859 and Fermilab, operated by Fermi Research Alliance, LLC under Contract No. DE-AC02-07CH11359 with the United States Department of Energy, and gratefully acknowledges the Aspen Center for Physics, which is supported by National Science Foundation Grant No. PHY-1066293, where part of this work was performed. B. S. is supported by the DOE under Grants No. DE-SC0007859 and No. DE-SC0011719. K. Z. is supported by the DOE under Contract No. DE-AC02-05CH11231.

APPENDIX: DETAILS OF NUMERICAL METHODS

When solving the Einstein equations, for the metric initial data we use a conformally flat spatial metric $\gamma_{ij} = \Psi^4 f_{ij}$ and set the trace of the extrinsic curvature according to the inflationary Hubble parameter $K = -3H$, while fixing the traceless part to be zero. With these choices, the momentum constraint is trivially satisfied, while the Hamiltonian constraint is solved using the code described in [60] to obtain the conformal factor Ψ. In practice, since we consider cases with $h_{\rm in} \ll h_{\rm min}$, the conformal factor is always close to unity, and hence the initial metric is very nearly just a slice of de Sitter in planar coordinates.

We evolve the Einstein field equations in the generalized harmonic formulation as described in [61,62]. In this formulation, the coordinate degrees of freedom are specified through the source functions $\Box x_a = H_a$. Here we fix the source functions to be those of the inflationary de Sitter metric: $H_t = 3H$ and $H_i = 0$. We use compactified coordinates that extend to spatial infinity where we impose the boundary condition that the metric be exactly de Sitter. Hence, away from any regions with large Higgs field fluctuations or potential energy, the coordinates $\{t, x^i\}$ we use will very closely match de Sitter planar coordinates.

As in [63], we evolve both the metric and scalar field using fourth-order finite differences and fourth-order Runge-Kutta time stepping. We take advantage of the

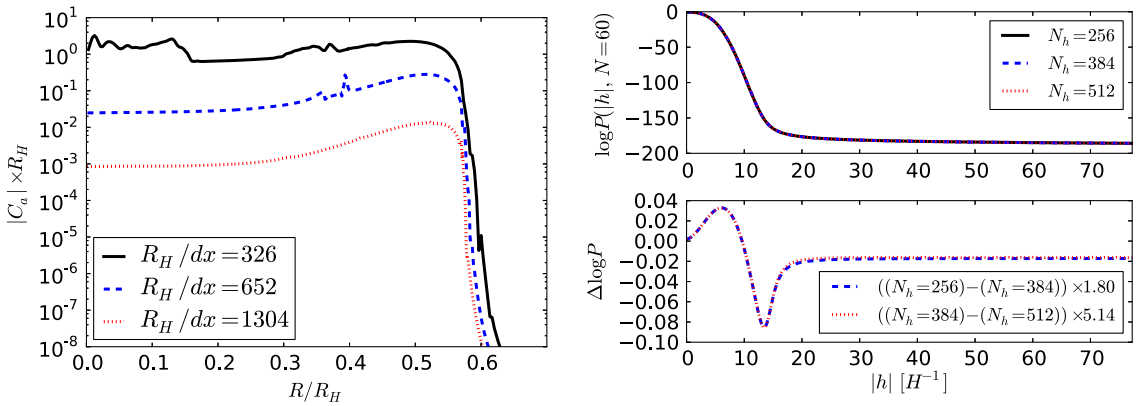

FIG. 11. Left panel: The norm of the Einstein equation constraint violation $C_a = \Box x_a - H_a$ for simulations at three different resolutions of the case shown in Fig. 2, at $tH = 0.78$ (just before the formation of a black hole). The scaling with resolution is consistent with approximately fourth-order convergence. Right panel: Solutions of the Fokker-Planck equation [Eq. (12)] for $H/\Lambda_{\rm max} = 0.07$ and $b_0 = 0.16/(4\pi)^2$ at $N = 60$ at three different resolutions (top), and the difference between the resolutions (bottom). In the latter case, the quantities are scaled to indicate the error in $\log P$ for the lowest resolution (which is used for the results in this paper), consistent with second-order convergence.

axisymmetry of the problem to make the computational grid a half-plane while still using Cartesian coordinates through the use of a modified Cartoon method as described in [61]. To eliminate numerical error coming from just evolving the known de Sitter solution, we use the background error subtraction technique [64]. In the left panel of Fig. 11, we demonstrate the expected convergence for an example case. The results presented in this paper use the medium or high resolution shown there.

We solve the FP equation written in terms of the variable $X \equiv \log P$, Eq. (12), using standard second-order finite differences for the field derivatives, and the Crank-Nicholson method for the time integration—an implicit method often used for diffusion type equations. As an initial condition, we choose P to be a narrow Gaussian distribution with zero mean and variance given by Eq. (20) evaluated at $N = 1/8$. At the outer boundary, we impose the condition that $\partial X/\partial h = h(\partial^2 X/\partial^2 h)$, which is chosen to be compatible with a Gaussian initial condition. We have verified that our results are not sensitive to the placement of the outer boundary (at a few times $h_{s/r}$) or the exact width of the initial distribution. The numerical error and convergence for an example case are shown in the right panel of Fig. 11.

[1] M. Sher, Phys. Rep. **179**, 273 (1989).
[2] M. Sher, Phys. Lett. B **317**, 159 (1993).
[3] J. Casas, J. Espinosa, and M. Quiros, Phys. Lett. B **342**, 171 (1995).
[4] G. Altarelli and G. Isidori, Phys. Lett. B **337**, 141 (1994).
[5] J. Ellis, J. Espinosa, G. Giudice, A. Hoecker, and A. Riotto, Phys. Lett. B **679**, 369 (2009).
[6] J. Elias-Miró, J. R. Espinosa, G. F. Giudice, G. Isidori, A. Riotto, and A. Strumia, Phys. Lett. B **709**, 222 (2012).
[7] G. Isidori, V. S. Rychkov, A. Strumia, and N. Tetradis, Phys. Rev. D **77**, 025034 (2008).
[8] G. Isidori, G. Ridolfi, and A. Strumia, Nucl. Phys. **B609**, 387 (2001).
[9] F. Bezrukov, M. Yu. Kalmykov, B. A. Kniehl, and M. Shaposhnikov, J. High Energy Phys. 10 (2012) 140.
[10] G. Degrassi, S. Di Vita, J. Elias-Miró, J. R. Espinosa, G. F. Giudice, G. Isidori, and A. Strumia, J. High Energy Phys. 08 (2012) 098.
[11] D. Buttazzo, G. Degrassi, P. Paolo Giardino, G. F. Giudice, F. Sala, A. Salvio, and A. Strumia, J. High Energy Phys. 12 (2013) 089.
[12] P. Creminelli, D. L. Lpez Nacir, M. Simonović, G. Trevisan, and M. Zaldarriaga, J. Cosmol. Astropart. Phys. 11 (2015) 031.
[13] J. R. Espinosa, G. F. Giudice, and A. Riotto, J. Cosmol. Astropart. Phys. 05 (2008) 002.
[14] O. Lebedev and A. Westphal, Phys. Lett. B **719**, 415 (2013).
[15] A. Kobakhidze and A. Spencer-Smith, Phys. Lett. B **722**, 130 (2013).
[16] K. Enqvist, T. Meriniemi, and S. Nurmi, J. Cosmol. Astropart. Phys. 10 (2013) 057.
[17] A. Hook, J. Kearney, B. Shakya, and K. M. Zurek, J. High Energy Phys. 01 (2015) 061.
[18] K. Enqvist, T. Meriniemi, and S. Nurmi, J. Cosmol. Astropart. Phys. 07 (2014) 025.
[19] M. Herranen, T. Markkanen, S. Nurmi, and A. Rajantie, Phys. Rev. Lett. **113**, 211102 (2014).
[20] A. Kobakhidze and A. Spencer-Smith, arXiv:1404.4709.
[21] M. Fairbairn and R. Hogan, Phys. Rev. Lett. **112**, 201801 (2014).
[22] A. Shkerin and S. Sibiryakov, Phys. Lett. B **746**, 257 (2015).
[23] J. Kearney, H. Yoo, and K. M. Zurek, Phys. Rev. D **91**, 123537 (2015).
[24] J. R. Espinosa, G. F. Giudice, E. Morgante, A. Riotto, L. Senatore, A. Strumia, and N. Tetradis, J. High Energy Phys. 09 (2015) 174.
[25] B. Freivogel, G. T. Horowitz, and S. Shenker, J. High Energy Phys. 05 (2007) 090.
[26] M. C. Johnson and I.-S. Yang, Phys. Rev. D **82**, 065023 (2010).
[27] S. R. Coleman and F. De Luccia, Phys. Rev. D **21**, 3305 (1980).
[28] S. Hawking and I. Moss, Phys. Lett. **110B**, 35 (1982).
[29] K. S. Thorne, in *Magic Without Magic: John Archibald Wheeler*, edited by J. Klauder (Freeman, San Francisco, 1972), p. 231.
[30] A. D. Linde, Nucl. Phys. **B372**, 421 (1992).
[31] A. A. Starobinsky, Stochastic de sitter (inflationary) stage in the early universe, in *Field Theory, Quantum Gravity and Strings*, edited by H. J. de Vega and N. Sánchez (Springer Berlin Heidelberg, Berlin, Heidelberg, 1986), Vol. 246, pp. 107–126.
[32] F. Finelli, G. Marozzi, A. A. Starobinsky, G. P. Vacca, and G. Venturi, Phys. Rev. D **79**, 044007 (2009).
[33] A. A. Starobinsky and J. Yokoyama, Phys. Rev. D **50**, 6357 (1994).
[34] A. R. Brown and E. J. Weinberg, Phys. Rev. D **76**, 064003 (2007).
[35] Y. Sekino, S. Shenker, and L. Susskind, Phys. Rev. D **81**, 123515 (2010).
[36] S. W. Hawking and G. F. R. Ellis *The Large Scale Structure of Space-time* (Cambridge University Press, Cambridge, 1973), Vol. 1.
[37] S. A. Hayward, Phys. Rev. D **49**, 6467 (1994).
[38] J. P. S. Lemos, Phys. Lett. B **353**, 46 (1995).
[39] J. P. S. Lemos, Phys. Rev. D **57**, 4600 (1998).

[40] A. R. Liddle and S. M. Leach, Phys. Rev. D **68**, 103503 (2003).
[41] C. Cheung, M. Papucci, and K. M. Zurek, J. High Energy Phys. 07 (2012) 105.
[42] G. Aad *et al.* (ATLAS and CMS Collaborations), Phys. Rev. Lett. **114**, 191803 (2015).
[43] V. Khachatryan *et al.* (CMS Collaboration), Phys. Rev. D **93**, 072004 (2016).
[44] M. Aaboud *et al.* (ATLAS Collaboration), Phys. Lett. B **761**, 350 (2016).
[45] A. H. Hoang and I. W. Stewart, Nucl. Phys. B, Proc. Suppl. **185**, 220 (2008).
[46] S. Moch *et al.*, arXiv:1405.4781.
[47] P. A. R. Ade *et al.* (BICEP2 and Keck Array Collaborations), Phys. Rev. Lett. **116**, 031302 (2016).
[48] ATLAS, CDF, CMS, and D0 Collaborations, arXiv:1403.4427.
[49] C. Gross, O. Lebedev, and M. Zatta, Phys. Lett. B **753**, 178 (2016).
[50] K. Kamada, Phys. Lett. B **742**, 126 (2015).
[51] Y. Ema, K. Mukaida, and K. Nakayama, Phys. Lett. B **761**, 419 (2016).
[52] J. Garcia-Bellido, D. G. Figueroa, and J. Rubio, Phys. Rev. D **79**, 063531 (2009).
[53] M. Herranen, T. Markkanen, S. Nurmi, and A. Rajantie, Phys. Rev. Lett. **115**, 241301 (2015).
[54] Y. Ema, K. Mukaida, and K. Nakayama, J. Cosmol. Astropart. Phys. 10 (2016) 043.
[55] K. Kohri and H. Matsui, Phys. Rev. D **94**, 103509 (2016).
[56] K. Enqvist, S. Nurmi, and S. Rusak, J. Cosmol. Astropart. Phys. 10 (2014) 064.
[57] D. G. Figueroa, J. Garcia-Bellido, and F. Torrenti, Phys. Rev. D **92**, 083511 (2015).
[58] K. Enqvist, S. Nurmi, S. Rusak, and D. Weir, J. Cosmol. Astropart. Phys. 02 (2016) 057.
[59] K. D. Lozanov and M. A. Amin, J. Cosmol. Astropart. Phys. 06 (2016) 032.
[60] W. E. East, F. M. Ramazanoglu, and F. Pretorius, Phys. Rev. D **86**, 104053 (2012).
[61] F. Pretorius, Classical Quantum Gravity **22**, 425 (2005).
[62] W. E. East, F. Pretorius, and B. C. Stephens, Phys. Rev. D **85**, 124010 (2012).
[63] W. E. East, M. Kleban, A. Linde, and L. Senatore, J. Cosmol. Astropart. Phys. 09 (2016) 010.
[64] W. E. East and F. Pretorius, Phys. Rev. D **87**, 101502 (2013).